CHALMERS
UNIVERSITY OF TECHNOLOGY

Novel approach to recycling of steel swarf using hydrometallurgy

Resources, Conservation & Recycling 185 (2022) 106450

Contents lists available at ScienceDirect

Resources, Conservation & Recycling

journal homepage: www.elsevier.com/locate/resconrec

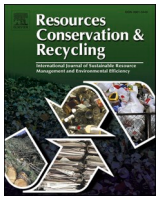

Full length article

Novel approach to recycling of steel swarf using hydrometallurgy

Thomas Ottink *, Nathalia Vieceli, Mark R.StJ. Foreman, Martina Petranikova

Department of Chemistry and Chemical Engineering, Industrial Materials Recycling, Chalmers University of Technology, Kemivägen 4, Gothenburg 41258, Sweden

ARTICLE INFO

Keywords:
Steel swarf
Recycling
Selective leaching
Cutting fluid
Ferric chloride
Hazardous waste

ABSTRACT

Steel swarf is a hazardous waste which is challenging to recycle due to its high content of heavy metals and cutting fluids and is today commonly landfilled. The swarf can contain up to 80% iron and represents a potential secondary raw material for production of reagents like ferric chloride, which can be utilized in wastewater treatment. This work presents a novel hydrometallurgical approach for recycling steel swarf and production of ferric chloride by selective separation of iron from heavy metals. Swarf containing 69% iron was leached with hydrochloric acid. A leachate containing 24.600 mg/L Fe with 150 mg/L Mn, 12 mg/L Ni and <1 mg/L Cr and Mo was obtained. The oil-based cutting fluids largely remained in the solid residue with only 1% dissolution in the aqueous phase. These findings showed that ferric chloride solutions of 99% purity can be produced from steel swarf in a single leaching step.

1. Introduction

Machining of steel products generates large amounts of ferrous swarf and other non-ferrous by-products. The exact amount of steel swarf produced annually is unknown but has been estimated to 2.3–5.8 million tons (Chang et al., 2006). Processes like milling, turning and grinding, commonly make use of cutting fluids to cool and lubricate metalworking equipment (el Baradie, 1996a), and generate an oil covered swarf. Steel producers are reluctant to process this swarf as scrap since combustible oils can produce flames and explosions, damaging processing equipment (Chang et al., 2006). Cutting fluids can also contain phosphorous and sulfur which can have an adverse effect on the quality of produced steel (Krauss, 2015). Recycling of metals from oil-covered swarf has had little economic feasibility and as such, swarf is today commonly deposited in landfills for hazardous waste (Forsgren, 2021).

Swarf from grinding operations has an especially complex composition and contains both cutting fluids and abrasives and binder material from the grinding wheel. The main constituent of this swarf is iron with a content of 50–80% (Irani et al., 2005). Besides iron, it can also contain various alloying elements from the steel like Cr, Mn and Mo, and between 4 and 20% of ceramic abrasives like alumina or silicon carbide. Cutting fluids are either synthetic or mineral oil-based and can contain several additives like biocides, rust inhibitors and extreme pressure agents (Wu et al., 2021). Many additives are toxic and have a low biodegradability. Thus, cutting fluids are regarded as a hazardous waste by the European Union (European Waste Catalogue, 12 01 07*). Partial separation of swarf from the grinding sludges is possible through filtration, magnetic separation or centrifugation (el Baradie, 1996b; Lee et al., 2017). However, residual swarf can still contain up to 50% cutting fluids (Chang et al., 2006).

Previous studies on recycling of swarf have primarily been focused on lowering the cutting fluid content. Extraction of the cutting fluids using supercritical carbon dioxide and aqueous washing of swarf with surfactants has so far received most attention (Chang et al., 2006; Fu et al., 1998; Lee et al., 2020; Ruffino and Zanetti, 2008). With these techniques, the cutting fluid content can usually be reduced below 5% which enables reprocessing of the swarf as scrap. Hankel et al. recently suggested washing swarf with alkaline surfactants and mechanically separating the ferrous fraction from abrasives (Hankel et al., 2020). With this approach, new steel can be produced directly by sintering the metallic swarf. Moreover, abrasive material could potentially be reused instead of ending up as slag at the steel mill. Steel produced by sintering however had low quality due to difficulties in separating swarf from abrasives.

Recycling of swarf using a hydrometallurgical approach has not yet been reported. Hydrometallurgy offers an energy efficient alternative to pyrometallurgical processes and can be used to recover metals from low grade ores and secondary resources (Tunsu et al., 2015). This technique has already seen application in recycling of other by-products from the steel industry (Binnemans et al., 2020). While most studies have been focused on the recovery of Zn from electric arc furnace dust, recycling of

* Corresponding author.
E-mail address: ottink@chalmers.se (T. Ottink).

https://doi.org/10.1016/j.resconrec.2022.106450
Received 5 April 2022; Received in revised form 1 June 2022; Accepted 7 June 2022
Available online 18 June 2022

valuable alloying elements like Mo and W has also recently gained some attention (Petranikova et al., 2020; Virolainen et al., 2013). Hydrometallurgy could potentially be used to selectively extract metals from swarf since oil-based cutting fluids have a low solubility in water.

The aim of this work was to achieve selective separation of metals from cutting fluid and abrasives by leaching. For this purpose, swarf was leached with dilute hydrochloric acid solutions while maintaining specific pH levels. This method has been applied previously for decontamination and recycling of a variety of different wastes like soils, MSWI ashes, flue dusts and slags (Cappuyns and Swennen, 2008). Hydrochloric acid can react with metals to form soluble chloride salts and since steel swarf has a high iron content, it can represent a raw material for production of ferric chloride ($FeCl_3$). Solutions of $FeCl_3$ are a marketable product and can be used as flocculants in wastewater treatment (Amuda and Amoo, 2007; Song et al., 2004). By providing an alternative application for the swarf, its potential value is increased. This promotes recycling and makes landfilling less attractive and thus brings a more sustainable solution for its handling.

2. Materials and methods

2.1. Material

Steel swarf samples were provided by Stena Recycling AB, Sweden. The swarf was generated by SKF in the production of ball bearings and was received as briquettes. Two briquettes were crushed into a dust using a mortar and pestle. Swarf was mixed by hand to create a representative sample and was stored in airtight polypropylene containers to prevent metals from oxidizing.

2.1.1. Metal and abrasive content

The content of leachable metals in the swarf was determined with Inductively Coupled Plasma-Optical Emission Spectroscopy (ICP-OES, Thermo Fisher, iCAP 6500) after digestion in aqua regia prepared using concentrated HNO_3 (65%, Merck, Suprapur) and HCl (37%, Sigma-Aldrich, ACS reagent). Swarf samples (0.2 g) were added to aqua regia (30 mL) and were leached for 2 h at 80 °C while stirring with a magnet at 300 rpm. Each solution was made up to 50 mL with Milli-Q water and filtered with polypropylene syringe filters (0.45 μm pore size). Filtrates were further diluted with 0.5 M HNO_3 and analyzed with ICP-OES.

The content of insoluble ceramic abrasives in the swarf was estimated by decomposing cutting fluids remaining in solid residues after digestion in aqua regia. A residue sample (0.4 g) was heated to 700 °C for 1 h in a muffle furnace and was thereafter weighed.

2.1.2. Cutting fluid and carbon content

The cutting fluid content was estimated by washing swarf samples in consecutive stages with toluene (≥99.5%, Sigma-Aldrich, ACS reagent), heptane (99%, Sigma-Aldrich, ReagentPlus®) and ethanol (95%, Solveco, Analytical grade). Swarf (2 g) was added to volumetric flasks and was washed by filling flasks with organic solution (50 mL) and mixing by shaking for 5 min. Liquid phase was decanted after 1 h when suspended solids had settled, which concluded a washing stage. Swarf was first washed in two stages with toluene to dissolve cutting oils. Next, three stages of washing with heptane followed by three stages with ethanol were performed to wash out toluene. Final ethanol solutions were filtered through glass microfiber filters (1.6 μm pore size, Whatman, GF/A grade) and filter papers with solid residue were dried in an oven at 60 °C for 24 h. The cutting fluid content was determined by comparing the mass of swarf samples before and after washing. The carbon content of swarf and leaching residues was determined with combustion analysis (LECO, CS744).

2.1.3. Crystalline composition

Crystalline compositions of swarf and leaching residues were determined with X-ray diffraction (XRD, Bruker, D8 advance). Samples were analyzed with a 2Θ angular range between 10° and 90°, step size of 0.04° and wavelength of 1.5406 Å. Diffraction peaks were against the International Center for Diffraction Data (ICDD) database.

2.2. Leaching experiments and optimization

Leaching experiments were performed in pairs in jacketed, 200 mL, glass reactors. A hot water flow from a bath to outer reactor shells was used to control leaching temperatures. Both reactors were equipped with glass electrodes for pH measurement and polypropylene burettes with anti-diffusion filters for titrations. Electric stirrers with polypropylene propellers operating at 1800 rpm were used to mix titrant and submerge the buoyant, oily swarf in leaching media. Electrodes and burettes from both reactors were connected to an automatic titrator (Metrohm, Titrando 905). The titrator was programmed with tiamo™ to monitor and control the pH of leaching solutions. Titrant was administered by 10 mL dosing units whenever the pH was above the desired level. A 5 M HCl solution was used as titrant in order to minimize dilution of leaching media.

Each reactor was initially filled with 100 mL Milli-Q water and preheated to the desired leaching temperature. A pre-titration was performed in order to start experiments at the desired pH level. Swarf samples were added to the reactors and leached while maintaining a constant pH level. Leachate samples were taken from reactors after a predetermined time and filtered with polypropylene syringe filters (0.45 μm pore size). Filtrate was diluted with 0.5 M HNO_3 and analyzed with ICP-OES. Metal concentrations were used to calculate leaching efficiencies EM using Eq. (1),

$$E_M(\%) = 100 \times \frac{C_{M,l} V_l}{m_s x_M} \quad (1)$$

where $C_{M,l}$ is the concentration of metal M in the leachate, V_l the volume of the leaching solution, m_s the mass of the original swarf sample and x_M the mass fraction of metal M in pure swarf. Thermodynamic data for leaching reactions and Eh-pH diagrams were generated with HSC Chemistry 9 (Outotec).

2.2.1. Design of experiments

Optimization of the leaching process was accomplished with design of experiments (DOE) and response surface methodology with calculations made in MATLAB. A detailed description of these methods is given by Montgomery (2020). Experiments were performed according to a face centered composite design (FCC, $\alpha = 1$) in order to avoid extreme conditions in axial points. Four replicates of the center point were used to estimate the experimental error. All experiments were performed in a random order and experimental pairs were assigned random reactors.

Effects of three factors were investigated: temperature (x_1), pH (x_2) and solid to liquid (S:L) ratio (x_3). Factor levels were selected based on results from preliminary leaching tests and Eh-pH diagrams and are presented in Table 2. The leaching time was set to 3 h and was based on the time for Cr to reach a steady concentration in preliminary leaching tests. Measured concentrations of Fe, Mn, Ni, Cr and Mo in the leachate were used to calculate leaching efficiency responses using Eq. (1).

Efficiency data for Fe, Cr, Mn and Ni was used to fit linear second order regression models with two- and three-way interaction terms, using the least squares method. The significance of regression models and regression coefficients was evaluated with hypothesis testing on 95% confidence bases and adjusted coefficients of determination (R^2_{adj}) were used to evaluate goodness of fit. Regression models were used to plot response surfaces for two factors while keeping one factor at a constant level.

2.3. Scale-up of leaching process

After optimizing the leaching process with DOE, a single large-scale

experiment was performed to validate the optimal conditions. Leaching was performed in a jacketed, 1 liter, glass reactor with a similar experimental setup as described in Section 2.2 Leaching experiments and optimization. The reactor was filled with 500 mL Milli-Q water which was preheated and pre-titrated. Swarf was added to the reactor and leached for 4 h while stirring at 300 rpm. Titrant was administered by a 20 mL dosing unit. Leachate samples of 1 mL were taken every hour and were filtered with 0.45 μm polypropylene syringe filters. Filtrate was diluted with 0.5 M HNO3 and analyzed with ICP-OES. After 4 h, leaching media was filtered through a 1.6 μm glass fiber filter using a vacuum filtration system. A filtrate sample was diluted 1:10 with 0.01 M HCl and analyzed with total organic carbon analysis (TOC, Shimadzu, 5050A).

2.3.1. Iron oxidation state determination

The oxidation state of dissolved Fe was determined with colorimetric analysis (Moss and Mellon 1942). A filtrate sample (0.5 mL) was diluted 1:2000 with 0.01 M HCl. Two 100 mL volumetric flasks were filled with 10 mL diluted sample each. Iron was reduced to Fe(II) in one flask by adding 2 mL, 10% hydroxylammonium chloride (≥99%, Merck, GR for analysis). A red coordination complex was formed with Fe^{2+} by adding 10 mL, 0.075% 2,2′-bipyridyl (≥99%, Sigma-Aldrich, ReagentPlus®) to both flasks. The solutions were stabilized with 10 mL, 50% ammonium acetate (≥97%, Sigma-Aldrich, ACS reagent) buffer, made up to 100 mL with Milli-Q water and mixed by shaking. After leaving the solutions to rest for 30 min, the Fe(II) content was determined with UV/VIS spectroscopy (PerkinElmer, Lambda 25) at a wavelength of 525 nm.

3. Results and discussion

3.1. Swarf characterization

The elemental composition of the swarf is given in Table 1: Elemental composition of the steel swarf. The main constituent of the swarf was Fe with a content of 69.3 wt%. Chromium (1.35%) was also present in the swarf as well as other alloying elements like Mn, Mo and Ni, which were found in lesser amounts (<1%). Combustion analysis showed that the swarf contained 5 wt% C which can be attributed mainly to organic carbon from the cutting oil since steel commonly contains <1% inorganic carbon (Krauss, 2015). After washing with toluene, heptane and ethanol, it was determined that the swarf contained at least 8.5 wt% cutting fluid. However, combustion analysis showed that washed swarf still contained 1.5% carbon and the cutting fluid content was likely somewhat higher.

The XRD patterns of pure swarf and leaching residues after dissolution in aqua regia with backgrounds subtracted are given in Fig. 1a and b respectively. The peaks observed at 2Θ values 43.2°, 65.4°, 82.2° for pure swarf correspond to body centered tetragonal α-Fe while peaks at 44.4°, 50.5°, 74.1° belong to face centered cubic γ-Fe. Carbon was incorporated into both crystalline structures (Fe_xC_y) and Fe was partially substituted by alloying elements (Fe_xM_{x-1}) (Krauss, 2015).

Several smaller peaks can be observed in at 25.4°, 35.0°, 37.7°, 57.4°, 66.4°, 68.1°, 76.5° and 80.8°, which belong to Al_2O_3. This is seen more clearly by comparison with Fig. 1b, where solid residues after dissolution in aqua regia were found to consist largely of alumina abrasives. Another smaller peak can be discerned at 18.1° in Fig. 1b, belonging to aluminium oxides with a spinel structure ($M_xAl_yO_4$). These likely come from impurities in the abrasive. The total content of abrasives was determined to be around 6 wt%.

A bump can be observed between 10 and 20° in Fig. 1a and b, which probably belongs to the amorphous cutting fluid. When dissolving swarf in aqua regia, most of the cutting fluid was oxidized, although some remained on the abrasive. Combustion analysis confirmed that the leaching residues contained 28 wt% carbon.

To summarize, the swarf had a high Fe content and could represent a source for production of iron chlorides. There was no evidence that it contained oxidized Fe. Besides Fe, the swarf also contained lesser amounts of Cr, Mn, Mo and Ni, which were soluble in aqua regia, and Al_2O_3 which was insoluble. The carbon content was relatively high and was mainly related to the cutting oil. The oil was highly persistent and was only partially eliminated when washing with toluene, heptane and ethanol.

Table 1
Elemental composition of the steel swarf. Variances are based on triplicate experiments.

Element	Content (wt%)	Element	Content (wt%)
Fe	69.3 ± 4.3	Mn	0.56 ± 0.01
C	5.05 ± 0.06	Mo	0.27 ± <0.01
Al	~3.3	Ni	0.09 ± <0.01
Cr	1.35 ± 0.02		

3.2. Leaching reactions and thermodynamics

The main constituent of the swarf was metallic Fe which can react with HCl in order to form iron chlorides via Eqs. (2) or (3).

$$Fe(s) + 2HCl(aq) \rightarrow FeCl_2(aq) + 2H_2(g) \quad (2)$$

$$Fe(s) + 3HCl(aq) \rightarrow FeCl_3(aq) + \frac{1}{2}H_2(g) \quad (3)$$

The reactions are irreversible and spontaneous with a standard Gibbs free energy of reaction of $\Delta G_r^o = -44.8$ kJ/mol and $\Delta G_r^o = -4.8$ kJ/mol respectively. Hydrogen is formed as a by-product in both reactions. In cases where the swarf contains considerable amounts of oxidized Fe, the leaching can also be described by Eqs. (4) or (5).

$$Fe_2O_3(s) + 6HCl(aq) \rightleftarrows 2FeCl_3(aq) + 3H_2O(l) \quad (4)$$

$$FeO(OH)(s) + 3HCl(aq) \rightleftarrows FeCl_3(aq) + 2H_2O(l) \quad (5)$$

Unlike the dissolution of metallic Fe, these reactions are reversible and non-spontaneous with $\Delta G_r^o = 21.8$ kJ/mol and $\Delta G_r^o = 11.4$ kJ/mol respectively. Precipitation of $FeCl_3$ via the reverse reactions is favored at high temperatures and low concentrations of HCl (Langová et al., 2009). According to Eh-pH diagrams, $FeCl_3$ is stable below pH 5 at 25 °C with a decreasing stability at higher temperatures.

3.3. Preliminary leaching tests

Preliminary leaching tests were performed to study the effects of pH and time on leaching of Fe and Cr. Leaching efficiencies for Fe and Cr at pH 2 and 4 and different leaching times are given in Fig. 2. Iron was more easily leached than Cr with final efficiencies of 82% Fe and 60% Cr at pH 2 and 73% Fe and 12% Cr at pH 4, after 6 h. This was predicted by Eh-pH diagrams which show that soluble Cr^{3+} is only stable below pH 1 at 25° Steady leachate concentrations of Fe were reached after 3 h at pH 2 but the dissolution was significantly slower at pH 4. This suggests that the leaching rate of Fe is limited by the concentration of HCl under the tested conditions. Steady concentrations of Cr were reached after leaching for 3 h regardless of pH. Preventing dissolution of Cr was a main priority in the process optimization and in order to study the leaching behavior of Cr, a fixed leaching time of 3 h was used in the experimental design.

3.4. Experimental design and response surfaces

Experimental conditions and responses obtained in the experimental design are given in Table 2. Experiments 1–8 correspond to the base 2^3 factorial design, 9–12 to center point experiments and 13–18 axial points of the FCC. Temperature and pH levels were selected based on the stability of $FeCl_3$. According to Eh-pH diagrams, $FeCl_3$ is stable below pH 4.2 at 60 °C. Due to operating close to the stability limit at combinations of high temperature and pH levels, some precipitation of Fe was

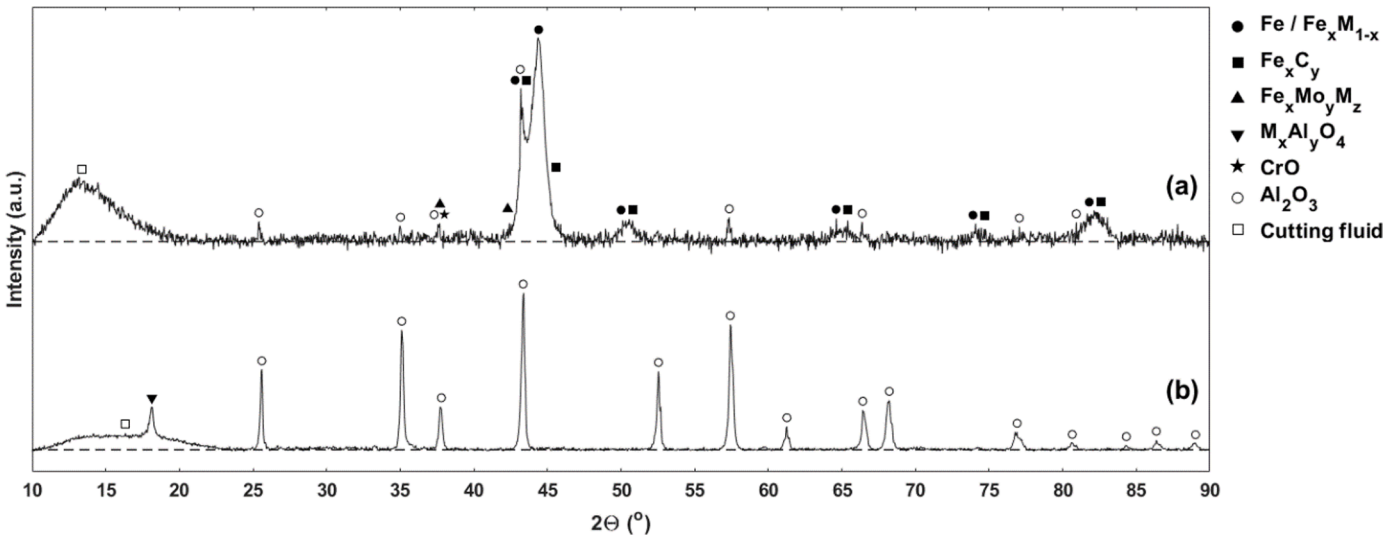

Fig. 1. XRD patterns of (a) pure swarf and (b) leaching residues after dissolution in aqua regia.

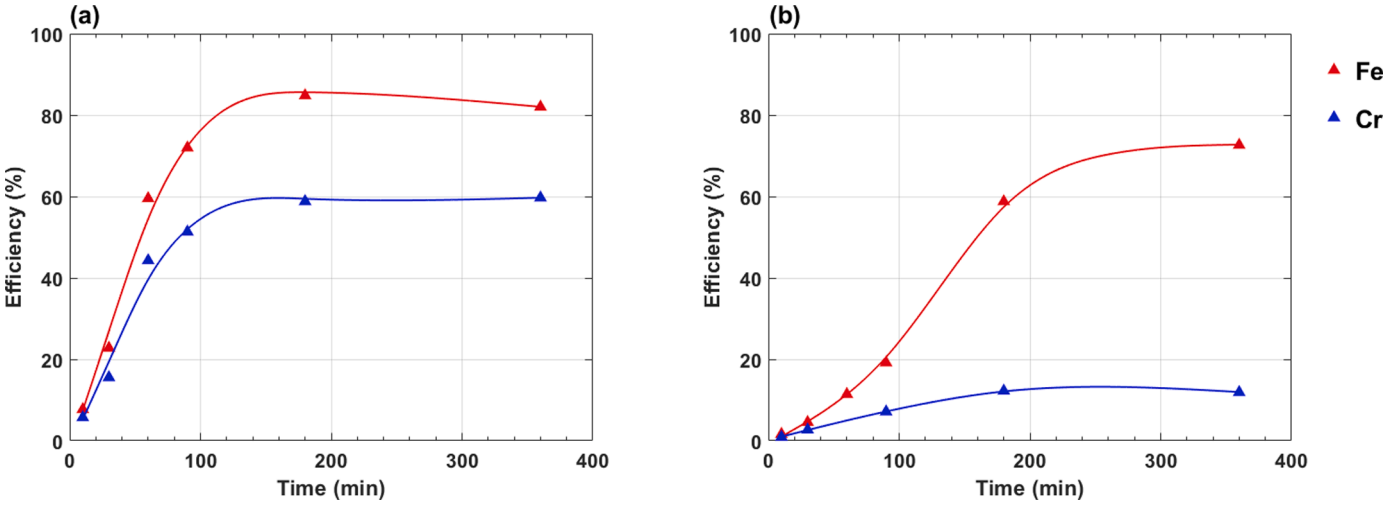

Fig. 2. Leaching efficiencies for Fe and Cr at various times when leaching swarf at (a) pH 2 and (b) pH 4. Conditions: 25 °C, S:*L* = 1:50 g/mL.

Table 2
Conditions used in the experimental design with leaching efficiency responses for Fe, Cr, Mn, Ni and Mo.

Random order	Standard order	Coded variables			Real variables			Response (leaching efficiency,%)				
		x_1	x_2	x_3	T (°C)	pH	S:L	Fe	Cr	Mn	Ni	Mo
11	1	-1	-1	-1	20	2	1:50	82	50	70	47	7
18	2	1	-1	-1	60	2	1:50	100	56	85	100	19
13	3	-1	1	-1	20	4	1:50	33	2	28	21	<LOD*
1	4	1	1	-1	60	4	1:50	87	<1	71	66	<LOD*
10	5	-1	-1	1	20	2	1:20	83	47	67	37	7
2	6	1	-1	1	60	2	1:20	100	57	86	87	9
8	7	-1	1	1	20	4	1:20	15	6	14	6	<LOD*
12	8	1	1	1	60	4	1:20	58	1	48	20	<LOD*
3	9	0	0	0	40	3	1:35	95	35	77	80	7
6	10	0	0	0	40	3	1:35	96	45	77	84	11
4	11	0	0	0	40	3	1:35	93	42	76	77	10
14	12	0	0	0	40	3	1:35	86	38	72	76	9
15	13	-1	0	0	20	3	1:35	58	33	51	25	2
7	14	1	0	0	60	3	1:35	96	21	80	100	4
17	15	0	-1	0	40	2	1:35	93	54	78	94	11
5	16	0	1	0	40	4	1:35	67	5	55	44	<LOD*
9	17	0	0	-1	40	3	1:50	96	45	79	100	12
16	18	0	0	1	40	3	1:20	88	36	72	49	7

*LOD = limit of detection.

observed in experiments 4 and 8. Relatively low S:L ratios were chosen for the design, mainly to avoid decreasing the viscosity of the leaching media since this can inhibit the mixing and distribution of HCl.

3.4.1. Regression modelling and diagnostics

Regression models for leaching efficiencies of Fe, Cr, Mn and Ni are given in Eqs. (6)–(9). The models are valid within the boundaries of the experimental design. Responses for Fe, Mn and Cr were fitted with second order regression models with two- and three-way interactions. Responses for Ni were fitted with a reduced regression model without three-way interaction ($x_1x_2x_3$) or second order S:L ratio terms (x_3^2) in order to improve the quality of the model. Only statistically significant

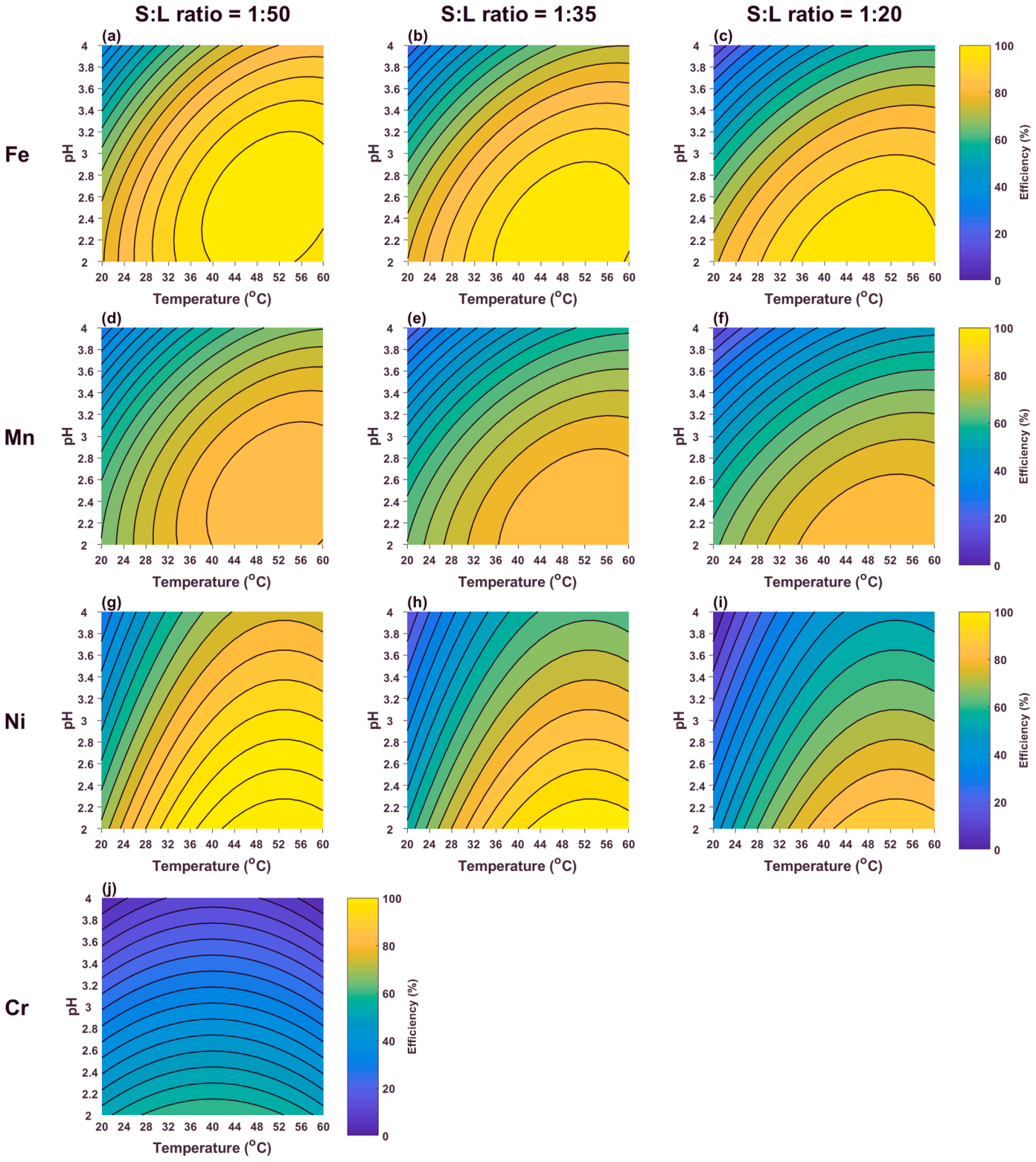

Fig. 3. : Contour plots of response surfaces for (a-c) Fe, (d-f) Mn, (g-i) Ni and (j) Cr for constant S:L ratios (a,d,g) 1:50 g/mL, (b,e,h) 1:35 g/mL and (c,f,i) 1:20 g/mL. The regression model for Cr was independent of x_3 and is valid for all S:L ratios in the experimental range.

terms are presented for each model. No model was generated for Mo since efficiencies were usually low and in several cases below the limit of detection (LOD) for ICP-OES.

$$E_{Fe} = 91.5 + 17.1x_1 - 19.8x_2 - 5.4x_3 + 7.6x_1x_2 - 5.9x_2x_3 - 13.1x_2^2 - 10.2x_2^2 \quad (6)$$

$$E_{Mn} = 75.0 + 14.1x_1 - 17.0x_2 - 4.6x_3 + 5.4x_1x_2 - 4.4x_2x_3 - 9.2x_1^2 - 8.3x_2^2 \quad (7)$$

$$E_{Ni} = 78.6 + 23.7x_1 - 20.7x_2 - 13.5x_3 - 18.2x_2^2 \quad (8)$$

$$E_{Cr} = 37.8 - 25.0x_2 - 8.9x_1^2 \quad (9)$$

Results from ANOVA for the regression models are given in Table S1. The significance of regression models and presence of lack of fit (LOF) was evaluated with *F*-tests ($\alpha = 0.05$). All regression models were significant ($F > F_{crit}$). Some LOF was present in the model for Ni and the model was improved by eliminating least significant terms in the regression model until the LOF was minimized.

Pareto charts with standardized regression coefficients are given in Figure S1. The significance of coefficients was evaluated with t-tests ($\alpha = 0.05$). Temperature (x_1) and pH (x_2) had the greatest influence on the leaching of Fe while S:L ratio (x_3) had a relatively low effect. The Pareto chart for Mn was almost identical to chart for Fe. A comparison of regression models in Eqs. (6) and (7), confirms that the models for Fe and Mn were similar. Thus, co-leaching of Mn is inevitable when leaching Fe. Leaching of Ni was mainly influenced by x_1 and x_2, however x_3 also had a comparably high effect. This presented a possibility to control the dissolution of Ni without greatly affecting leaching of Fe. The leaching of Cr was independent of x_3 and almost exclusively influenced by x_2.

Observed responses in the experimental design versus responses predicted by the regression models are given in Fig. S2. Regression models for Fe, Mn and Cr fitted experimental data well with R^2_{adj} close to 1. The R^2_{adj} for Ni (0.86) was slightly lower and the model did not fit experimental data with efficiencies close to 0 and 100% well. This was likely the reason for LOF in the ANOVA and the model for Ni should be used with some caution.

3.4.2. *Response surfaces and process optimization*

Optimization of the leaching process was accomplished with response surface methodology. Response surfaces were created by calculating leaching efficiencies using the regression models in Eqs. (6)–(9), at different temperature and pH levels while keeping the S:L ratio constant at the low ($x_3 = -1$), intermediate ($x_3 = 0$) and high ($x_3 = 1$) levels. Contour plots of response surfaces are given in Fig. 3.

Contour plots for Fe in Fig. 3a–c show that leaching efficiencies close to 100% were generally achievable within 3 h between pH 2–3 and 40 °C-60 °C. A maximum in leaching efficiency was predicted at 50 °C and pH levels between 2 and 2.5, depending on the S:L ratio. When increasing the S:L ratio, the ratio of metals to acid increases which can limit reaction kinetics. This behavior was also observed when comparing pH levels in the preliminary tests in Fig. 2 and explains the relatively low efficiencies for Fe at pH 4 and 20 °C after 3 h.

Leaching rates and efficiencies for Fe could be improved by operating at a higher temperature. Contour plots show that predicted efficiencies at pH 4 were generally 50% higher when operating at 60 °C compared to 20 °C. Likewise, at pH 2 only 80% of Fe could be leached at 20 °C while efficiencies were 100% at temperatures above 40 °C. According to the preliminary test in Fig. 2a, the Fe concentration reached a steady level after 3 h at pH 2 and 25 °C. This implies that only 80% of Fe was leachable when operating at 20 °C. Remaining Fe was likely trapped in the solid residue with Cr. Chromium oxides act as stabilizers in steel and are impervious to dilute HCl solutions (Krauss, 2015).

The leaching behavior of Mn was almost identical to that of Fe which is evident from similarity between contour plots in Fig. 3a–f. While this made co-leaching of Mn difficult to prevent, contour plots also show that a 5–15% lower efficiency for Mn could be expected compared to Fe.

Leaching of Ni was highly temperature dependent which is clear from the steep efficiency gradient between 20 °C and 40 °C in Fig. 3g–i. Maximum leaching efficiencies were predicted at 50 °C and pH 2. Comparing contour plots for Ni shows that S:L ratio also had a relatively high effect. The regression model for Ni in Eq. (8), shows that leaching of Ni decreased linearly with x_3 and predicted efficiencies for Ni were generally 25–30% lower at 1:20 than 1:50 g/mL.

Leaching of Cr increased linearly with decreasing pH and was independent of the S:L ratio. Temperature also had a minor effect which is shown by the curvature of the contour lines in Fig. 3. The regression model predicted a minimum efficiency of 4% at pH 4 and 20 °C and 60 °C. Leaching of Cr was inhibited with a higher temperature. This becomes evident when comparing experimental pairs (3,4), (7,8) and (13,14) in Table 2, where temperature was the only varied factor. The Eh-pH diagrams also indicate that Cr^{3+} is less stable at high temperatures.

In order to optimize the leaching process, contour plots were compared. Given enough time, Fe could generally be leached with high efficiencies according to preliminary tests in Fig. 2. The leaching behavior of Mn was identical to that of Fe and was not considered in the optimization. Therefore, the highest priority was to minimize co-leaching of Cr and Ni.

Leaching of Cr was minimized at 60 °C and pH 4. Operating at a high temperature favored the leaching of Ni however, this metal had a far lower content in the swarf. High temperatures also improved the leaching rate and efficiency for Fe. At 60 °C and pH 4, leaching of Ni was minimized by operating at 1:20 g/mL. Predicted efficiencies for both Fe and Ni were 25% lower at this S:L ratio than 1:50 g/mL. For Fe, this was explained by limitations in reaction kinetics but there was no evidence that S:L ratio had an effect on the leachability. For Ni however, efficiencies generally decreased with increasing S:L ratio regardless of pH and temperature. Thermodynamic calculations show that the formation of $NiCl_2$ from Ni and HCl is spontaneous with $\Delta G_r^o - 45.8$ kJ/mol, and that Ni^{2+} is stable below pH 4.7 at 60 °C. Comparison with the ΔG_r^o for Fe in Eq. (2), gives no evidence that Ni is more difficult to leach than Fe. It is however obvious that Ni is less favored than Fe in a competition for HCl. Operating at high S:L ratios also results in better pre-concentration of $FeCl_3$ which is desirable from an industrial perspective.

To summarize, optimal conditions with predicted efficiencies of 4% Cr and 50% Ni were determined to be 60 °C, pH 4 and S:*L* = 1:20 g/mL. At these conditions, predicted efficiencies for Fe and Mn were 62% and 51% respectively and could potentially reach higher levels with a longer leaching time. According to the experimental results in Table 2, no leaching of Mo was expected to occur.

3.5. *Validation of optimal leaching conditions and solid residues*

A single large-scale leaching experiment was performed in order to test the optimal conditions. The leaching time was extended to 4 h to determine if more Fe could be extracted with an additional hour of leaching. Leaching efficiencies for metals every hour and XRD analysis of leaching residues are given in Fig. 4. According to Fig. 4a, steady leachate concentrations of Fe were not reached within 3 h and a final efficiency of 83% was achieved with an extra hour of leaching. Efficiencies for Fe and Mn were 10% higher and Ni 20% lower than predicted by the regression models after 3 h. These results could not be explained by the regression models or heterogeneity of the swarf and were likely related to mixing effects. In the small reactors, a stirring rate of 1800 rpm was required to create a vortex in order to submerge and mix the oil covered swarf while a rate of 300 rpm was sufficient in the large-scale setup. A build-up of swarf between the pH electrode and mixer shaft was also observed when operating at S:*L* = 1:20 g/mL in small reactors. Overall, contacting of swarf with acid was likely more

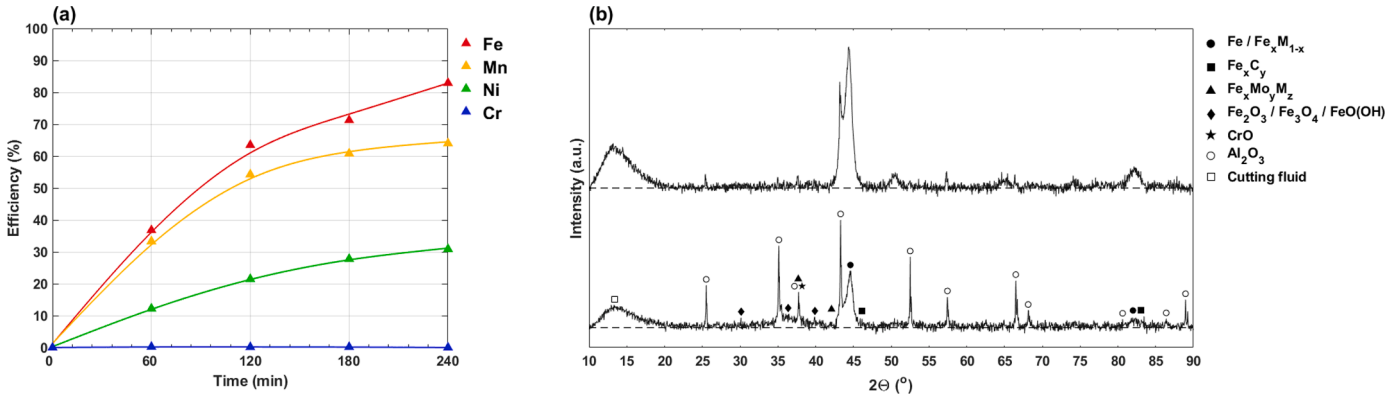

Fig. 4. : Characterization of leaching products in the large-scale leaching experiment: (a) efficiencies for metals during leaching with samples taken every hour and (b) XRD pattern of solid leaching residues (bottom) and pure swarf (top).

efficient in the large-scale experiment which can favor both reaction rates and selectivity (Paul et al., 2003). Efficiencies for Cr remained below 1% throughout the experiment and no Mo was detected. A mass balance for carbon showed that only around 1% of cutting fluid was dissolved during leaching and no secondary liquid phase was observed in the leachate through visual inspection of the filtrate. Leaching residue contained 7.2% carbon, thus most of the cutting oil remained in the solids.

Solid leaching residues had a dark brown color which indicated that Fe oxides were formed either during leaching or filtration. This was confirmed with XRD analysis and peaks for Fe_2O_3, Fe_3O_4 and FeO(OH) were observed at 2Θ-values 30.1°, 36.4° and 39.9° in Fig. 4b. Peaks for Fe/Fe_xM_{1-x} and Fe_xC_y at 43.2°, 44.6°, 50.5°, 65.4°, 74.1° and 82.4° were relatively small or no longer visible after leaching. This shows that most metallic Fe had been dissolved.

3.5.1. *Filtration and evaluation of leachate composition*

After leaching, the leachate was filtered and the carbon concentration in the filtrate was measured with TOC. Metal and carbon concentrations in the leachate before and after filtration are given in Table S2. A solution containing 24.600 mg/L Fe and <1 mg/L Cr and Mo was obtained after 4 h. The purity of iron chlorides was 99.3% on a trace metal basis, with 154 mg/L Mn and 12 mg/L Ni. The filtrate also contained 23 mg/L carbon which can be assumed to come from the organic cutting fluid.

Filtrate initially had a turquoise color typical for $FeCl_2$ solutions and colorimetric analysis confirmed that 96% of iron was Fe(II). Thermodynamic calculations show that $\Delta G_r^o = 0$ kJ/mol for the formation of $FeCl_3$ via Eq. (3) at 60 °C. This means that dissolution of Fe could only occur by formation of $FeCl_2$ via Eq. (2). Within 5 min after filtration, the solution adopted a yellow tone and the turbidity increased, indicating precipitation of Fe. The solution was stabilized, and solids were redissolved by adding 5 M HCl and lowering the pH to 1. Over the course of several days, the pH gradually increased, and the stabilized solution changed color from turquoise to yellow, typical for $FeCl_3$ solutions. Oxidation of $FeCl_2$ can occur via Eq. (10) and is spontaneous with $\Delta G_r^o = -330.8$ kJ/mol but slow.

$$4FeCl_2(aq) + 4HCl(aq) + O_2(aq) \rightleftarrows 4FeCl_3(aq) + 2H_2O(l) \quad (10)$$

A loss of 3000 mg/L Fe was observed between leaching and filtration while concentrations of other metals were unchanged. Consumption of HCl by leaching reactions continued after stopping the leaching experiment and resulted in an increased pH. This caused Fe to precipitate and can account for the Fe oxides found in the leaching residues. When operating close to the precipitation limit of Fe, immediate separation and stabilization of the filtrate with HCl is vital in order to prevent a loss of iron chlorides.

4. Conclusion

The leaching behavior of metals in steel swarf was investigated in diluted HCl solutions and a selective leaching process for the production of ferric chloride was developed and optimized. Approximately 99% of the cutting fluid stayed in the solid residue.

Swarf containing 69% metallic Fe, 1.4% Cr, lesser amounts of Mn, Mo and Ni and 6% alumina abrasives was target of the investigation. Complete dissolution of Fe was possible within 3 h when leaching between 40 °C and 60 °C and pH 2–3. The S:L ratio did not have an obvious effect on the leachability of Fe. The leaching behavior of Mn was identical to Fe. Leaching of Ni was clearly affected by S:L ratio with lower efficiencies at high S:L ratios. Leaching of Cr and Mo is governed by pH and minimal dissolution of these metals was achieved at pH 4. At this pH, temperature also has a minor influence on Cr with slightly less dissolution at 60 °C than 20 °C.

Optimal leaching conditions for production of ferric chloride were determined to be 60 °C, pH 4 and 1:20 g/mL. A leachate containing 24.600 mg/l Fe and 150 mg/l Mn and 12 mg/l Ni was obtained when leaching for 4 h. This corresponds to a 99.3% purity of iron chlorides on a trace metal basis. Only 1% of the cutting fluid was dissolved during leaching and solid residues were rich in oil, Cr, Mo and alumina. Further research will be conducted in order to further purify the obtained $FeCl_3$ solution and to investigate possible applications for the solid residue.

This work offers a novel approach to selective separation of metals from cutting fluids and abrasives in steel grinding swarf, which is today largely landfilled as a hazardous waste. It also shows how a low value waste can be utilized for production of a marketable product.

CRediT authorship contribution statement

T. O. wrote the paper, performed experiments, and analyzed the data. N.V. and M.P contributed with supervision and editing and reviewing of the manuscript. M. F. provided experimental procedures for iron state determination and washing of swarf. M.P. provided funding for the project.

Declaration of Competing Interest

The authors declare that they have no known competing financial interests or personal relationships that could have appeared to influence the work reported in this paper.

Acknowledgments

This research was supported by Formas (2021–00449). The authors would like to thank Chalmers Materials Analysis Laboratory (CMAL) for lending access to their facilities and Burçak Ebin for assisting with XRD

analysis and data interpretation. The authors also like to thank Stena Recycling for their cooperation and for providing swarf samples.

Supplementary materials

Supplementary material associated with this article can be found, in the online version, at doi:10.1016/j.resconrec.2022.106450.

References

Amuda, O.S., Amoo, I.A., 2007. Coagulation/flocculation process and sludge conditioning in beverage industrial wastewater treatment. J. Hazard. Mater. 141, 778–783. https://doi.org/10.1016/J.JHAZMAT.2006.07.044.

Binnemans, K., Jones, P.T., Manjón Fernández, Á., Masaguer Torres, V., 2020. Hydrometallurgical processes for the recovery of metals from steel industry by-products: a critical review. J. Sustain. Metall. 6 (4), 505–540. https://doi.org/10.1007/S40831-020-00306-2.

Cappuyns, V., Swennen, R., 2008. The application of pHstat leaching tests to assess the pH-dependent release of trace metals from soils, sediments and waste materials. J. Hazard. Mater. 158, 185–195. https://doi.org/10.1016/J.JHAZMAT.2008.01.058.

Chang, J.I., Lin, J.J., Huang, J.S., Chang, Y.M., 2006. Recycling oil and steel from grinding swarf. Resour. Conserv. Recycl. 49, 191–201. https://doi.org/10.1016/J.RESCONREC.2006.03.014.

el Baradie, M.A., 1996a. Cutting fluids: part I. Characterisation. J. Mater. Process. Technol. 56, 786–797. https://doi.org/10.1016/0924-0136(95)01892-1.

el Baradie, M.A., 1996b. Cutting fluids: part II. Recycling and clean machining. J. Mater. Process. Technol. 56, 798–806. https://doi.org/10.1016/0924-0136(95)01893-X.

Forsgren, C., 2021. Personal communication.

Fu, H., Matthews, M.A., Warner, S., 1998. Recycling steel from grinding swarf. Waste Manag. 18, 321–329. https://doi.org/10.1016/S0956-053X(98)00042-7.

Hankel, J., Jäger, S., Weber, S., 2020. Development of a recycling strategy for grinding sludge using supersolidus liquid phase sintering. J. Clean. Prod. 263, 121501 https://doi.org/10.1016/j.jclepro.2020.121501.

Irani, R.A., Bauer, R.J., Warkentin, A., 2005. A review of cutting fluid application in the grinding process. Int. J. Mach. Tools Manuf. 45, 1696–1705. https://doi.org/10.1016/J.IJMACHTOOLS.2005.03.006.

Krauss, G., 2015. Steels: Processing, Structure, and Performance, 2nd ed. ASM International.

Langová, Š., Leško, J., Matýsek, D., 2009. Selective leaching of zinc from zinc ferrite with hydrochloric acid. Hydrometallurgy 95, 179–182. https://doi.org/10.1016/J.HYDROMET.2008.05.040.

Lee, C.M., Choi, Y.H., Ha, J.H., Woo, W.S., 2017. Eco-friendly technology for recycling of cutting fluids and metal chips: a review. Int. J. Precis. Eng. Manuf. Green Technol. 4 (4 4), 457–468. https://doi.org/10.1007/S40684-017-0051-9.

Lee, H., Jung, M., Bae, M., Lee, E., Jin, H., Mishra, B., 2020. Removal of oil from ferrous grinding swarf of automobile industry by aqueous washing process. Waste Manag. 111, 51–57. https://doi.org/10.1016/J.WASMAN.2020.05.020.

Montgomery, D.C., 2020. Design and Analysis of Experiments, 10th ed. John Wiley & Sons.

Paul, E.L., Atiemo-Obeng, V.A., Kresta, S.M., 2003. Handbook of Industrial Mixing: Science and Practice. John Wiley & Sons.

Petranikova, M., Ssenteza, V., Lousada, C.M., Ebin, B., Tunsu, C., 2020. Novel process for decontamination and additional valorization of steel making dust processing using two-step correlative leaching. J. Hazard. Mater. 384, 121442 https://doi.org/10.1016/j.jhazmat.2019.121442.

Ruffino, B., Zanetti, M.C., 2008. Recycling of steel from grinding scraps: reclamation plant design and cost analysis. Resour. Conserv. Recycl. 52, 1315–1321. https://doi.org/10.1016/J.RESCONREC.2008.07.012.

Song, Z., Williams, C.J., Edyvean, R.G.J., 2004. Treatment of tannery wastewater by chemical coagulation. Desalination 164, 249–259. https://doi.org/10.1016/S0011-9164(04)00193-6.

Tunsu, C., Petranikova, M., Gergorić, M., Ekberg, C., Retegan, T., 2015. Reclaiming rare earth elements from end-of-life products: a review of the perspectives for urban mining using hydrometallurgical unit operations. Hydrometallurgy 156, 239–258. https://doi.org/10.1016/J.HYDROMET.2015.06.007.

Virolainen, S., Salmimies, R., Hasan, M., Häkkinen, A., Sainio, T., 2013. Recovery of valuable metals from argon oxygen decarburization (AOD) dusts by leaching, filtration and solvent extraction. Hydrometallurgy 140, 181–189. https://doi.org/10.1016/J.HYDROMET.2013.10.002.

Wu, X., Li, C., Zhou, Z., Nie, X., Chen, Y., Zhang, Y., Cao, H., Liu, B., Zhang, N., Said, Z., Debnath, S., Jamil, M., Ali, H.M., Sharma, S., 2021. Circulating purification of cutting fluid: an overview. Int. J. Adv. Manuf. Technol. 117, 2565–2600. https://doi.org/10.1007/S00170-021-07854-1/TABLES/13.